PHILOSOPHICAL TRANSACTIONS OF THE ROYAL SOCIETY A MATHEMATICAL, PHYSICAL & ENGINEERING SCIENCES

Interstellar Gas Studies in the Balloon Ultraviolet

A. Boksenberg, B. Kirkham, E. Michelson, M. Pettini, B. Bates, P. P. D. Carson, G. R. Courts, P. L. Dufton and C. D. McKeith

Phil. Trans. R. Soc. Lond. A 1975 **279**, 303-316
doi: 10.1098/rsta.1975.0063

Phil. Trans. R. Soc. Lond. A. **279**, 303–316 (1975) [303]
Printed in Great Britain

Interstellar gas studies in the balloon ultraviolet

By A. Boksenberg, B. Kirkham, E. Michelson and M. Pettini,
Department of Physics and Astronomy, University College London, S.W.7

B. Bates, P. P. D. Carson, G. R. Courts, P. L. Dufton and C. D. McKeith
Department of Pure and Applied Physics, The Queen's University of Belfast, Northern Ireland

[Plates 11 and 12]

Spectral observations at a resolution of 0.1 Å covering the region 2870–2740 Å have been made of several stars with an objective grating spectrograph mounted on a balloon-borne star-stabilized platform.

We report our measurements of the interstellar lines of Mg II at 2795.53 Å and 2802.70 Å and Mg I at 2852.13 Å. There are two important astrophysical reasons for observing these interstellar lines. First, in the general (H I) interstellar medium, Mg is predominantly in the Mg^+ state, so its interstellar abundance can be determined directly from the Mg II lines if the position on the curve of growth is known. Second, observation of both Mg^+ and Mg^0 gives information on the ionization balance and leads to a value for the interstellar electron density.

Values for the interstellar Mg abundance and electron density are derived for the gas in the directions of the stars observed. The results indicate that the predominant ionizing mechanism in cool clouds is photoionization by starlight.

Introduction

We present the results of spectral observations of interstellar Mg in the Mg II doublet lines 2795.5 Å and 2802.7 Å and the Mg I line 2852.1 Å, made in the directions of stars in Orion, Scorpius and Virgo. The astrophysical importance of such observations is well known. Since, in the general interstellar medium, Mg is predominantly in the Mg^+ state the column density of Mg can be determined directly from observations of the Mg II lines. Furthermore, observations of both Mg^+ and Mg^0 give information on the ionization balance and a figure for the interstellar electron density can be derived using appropriate estimates of the radiation field.

The observations were made from a balloon-borne payload, prepared jointly by University College London and The Queen's University, Belfast, in two flights in October 1972 (Bosenberg *et al.* 1972, 1974) and May 1973. The launches were carried out from the National Center for Atmospheric Research (NCAR) Balloon Flight Station, Palestine, Texas, using balloons of 0.57×10^6 m^3 capacity. In each flight the payload reached a float altitude about 40 km, at which the zenith atmospheric transmission is in the region of 50 % for the wavelength range of interest, and observations were carried out over a whole night.

The instrument

The payload consists of an altazimuth mounted primary star pointing platform carrying a high resolution objective grating spectrograph with an associated secondary fine-guidance system. The latter stabilizes the spectrum image to a few arcseconds in the direction of dispersion. First, coarse stabilization of the platform to about 1′ peak to peak is achieved with the

aid of an attached star sensor, which is directed to the tracked stars by ground command using a magnetometer for sensing the azimuth direction, and by reference to the local vertical. A second star sensor, in the fine-guidance system, provides an error signal for a secondary platform actuated in one axis and containing two folding mirrors which pass the incident starlight both into the fine star sensor and into a spectrograph mounted side by side. A simplified cutaway view of the system is shown in figure 1. The spectrograph has an objective plane grating of 2160 grooves per millimetre and ruled area 102 mm × 128 mm, used in second order. A small-angle quartz prism preceding the servo mirror is used to separate out the unwanted orders.

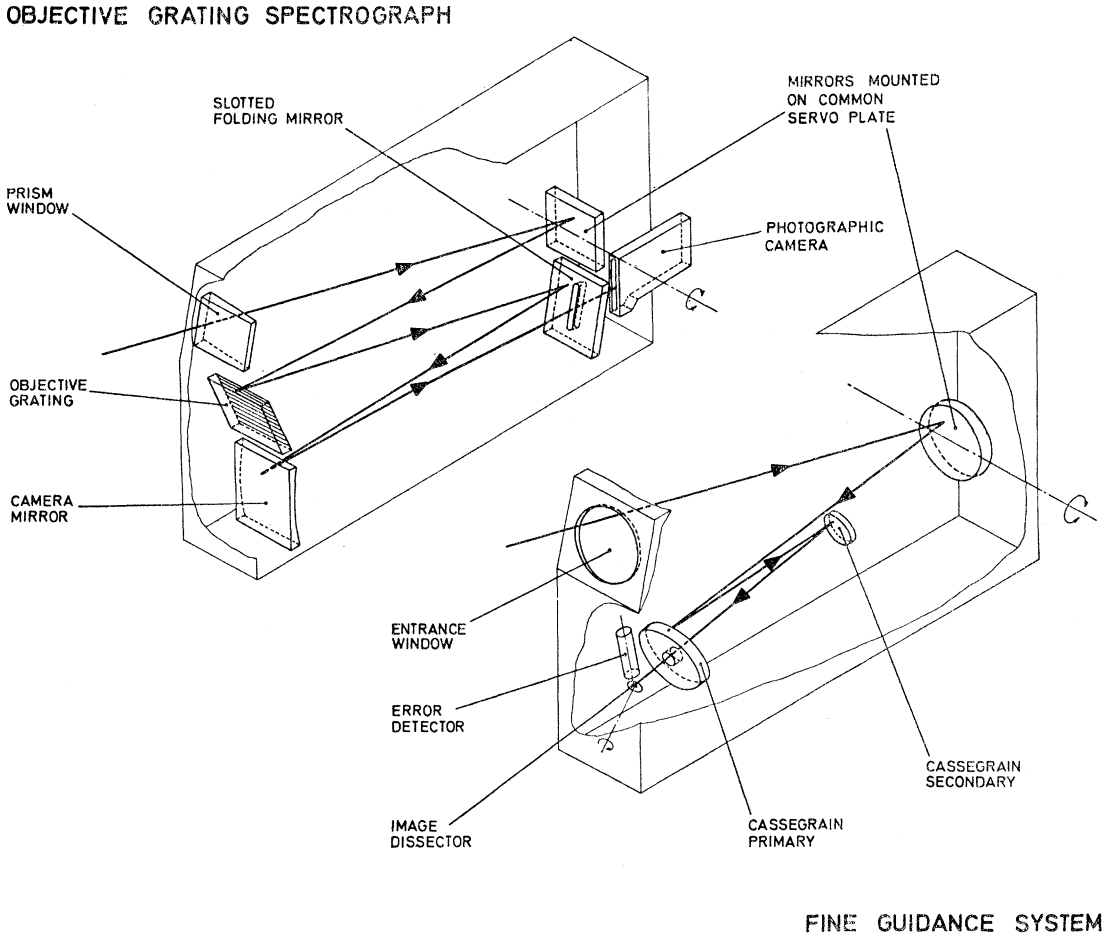

FIGURE 1. Diagrammatic view of the spectrograph and fine-guidance system. For clarity the two are shown separated.

The dispersed light from the grating is reflected from a plane slotted folding mirror to a spherical camera mirror used on axis, bringing the spectrum to a focus through the slot in the folding mirror. The spectral recordings are made on 103a-O roll film, wound on by telemetry command. The instrument covers the spectral range 2880–2730 Å with a spectral resolution better than 0.1 Å, governed almost equally by the inherent optical performance and the fine pointing error. The spectrograph was built and calibrated at Q.U.B. and the primary platform and fine-guidance system were built at U.C.L.

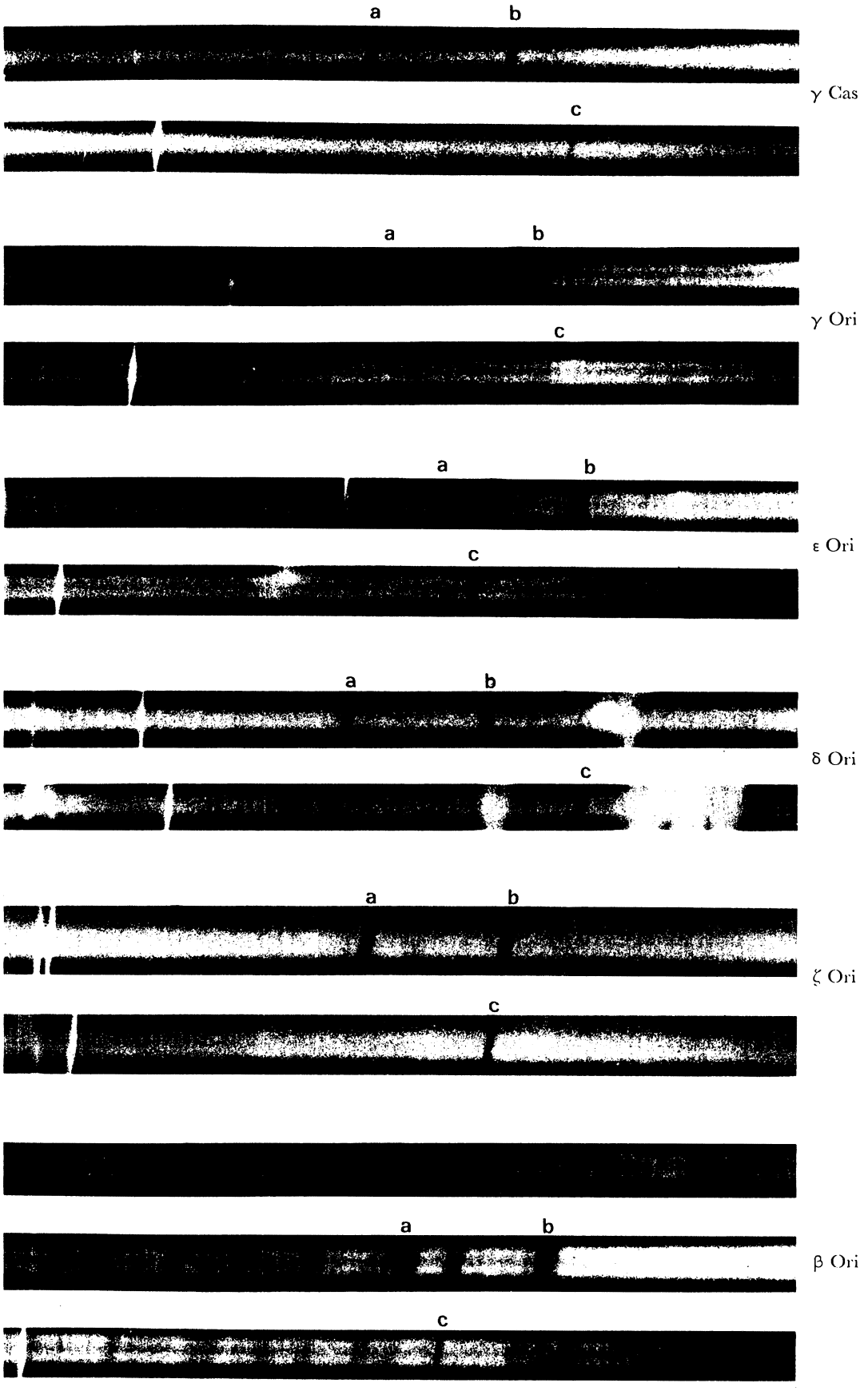

FIGURE 2. Segments of spectra of the stars observed in October 1972, showing the Mg II and Mg I interstellar lines (*a*, Mg II K; *b*, Mg II H; *c*, Mg I).

(*Facing p.* 304)

PHILOSOPHICAL TRANSACTIONS OF THE ROYAL SOCIETY A MATHEMATICAL, PHYSICAL & ENGINEERING SCIENCES

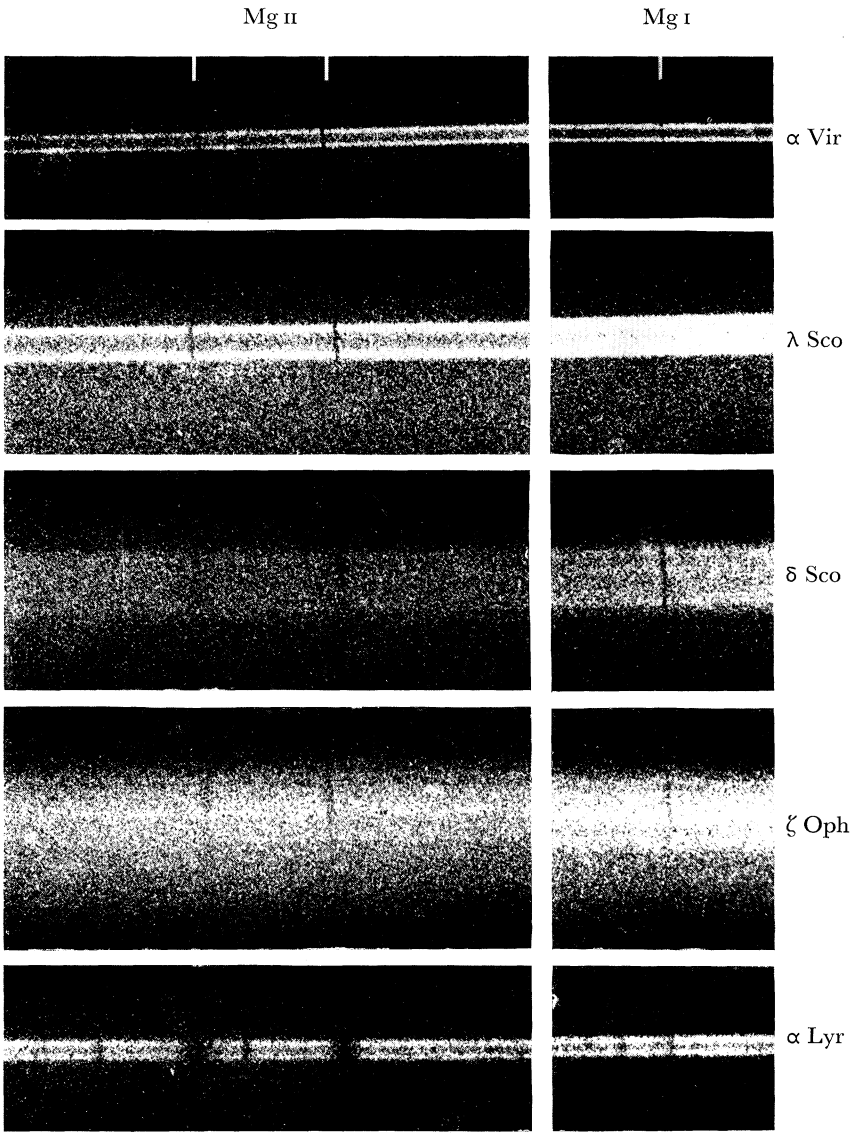

FIGURE 3. Segments of spectra of the stars observed in May 1973.

PHILOSOPHICAL TRANSACTIONS OF THE ROYAL SOCIETY A MATHEMATICAL, PHYSICAL & ENGINEERING SCIENCES

Flight data

Sample portions of the photographic spectra of the stars observed in the flight of October 1972 are shown in figure 2, plate 11. The spectra are widened by the motion of the pointing system, which is fine-stabilized only in the direction of dispersion. Apart from the bright fiducial mark to the left of the Mg I line, the bright trails and smudges present are undispersed images of nearby field stars: they caused no problem in the reduction of the interstellar data. The hotter of the observed stars show very little inherent spectral structure in the wavelength range covered, and the interstellar Mg II and Mg I lines stand out clearly. The cooler stars do show strong inherent spectral features, but the interstellar components easily are recognized by their relative strengths and shapes. Interstellar data in line to γ, δ, ϵ and ζ Ori are discussed below.

The sample spectra shown in figure 3 were recorded on the flight of May 1973. Better light baffling here excluded the stray images. Unfortunately, the flight ended in mishap with the loss of the entire payload in the Gulf of Mexico. (The complete payload now has been rebuilt and was successfully flown in May 1974.) After some 13 days' immersion in seawater the remains of the payload, including the flight emulsion in its camera housing, were accidentally recovered by a shrimp boat. As can be seen in figure 3, plate 12, the effect on the emulsion of the long soaking in seawater was to increase the fog level and grain noise. A great deal of effort then was expended in obtaining an appropriately simulated calibration for the modified emulsion, and we now have useful quantitative data for δ and λ Sco, α Vir and α Lyr and some qualitative data for ζ Oph. Because of the important part played by the calibration procedure, we consider it worth briefly describing this here.

The Kodak 103a-O emulsion with rem-jet backing is in 16 mm roll film form and in the spectrograph is contained in a light-tight camera assembly. On completion of a night's observing, unused film is wound tightly on to the take-up spool to give some additional protection against light leakage in the event of damage from a hard landing. In this flight, this procedure probably helped considerably in reducing the rate of chemical attack on the part of the film containing data. On recovery from the sea, the camera was kept in cold, clean water until the film was developed in the U.K. some 72 h later.

After carrying out tests on strips from the flight emulsion, a development time of 2.5 min in Kodak D 19 developer at a temperature of 19 °C was adopted. These conditions gave a useful density in the spectra and, at the same time, kept the background fog to a tolerable level. Even so, we found the background density level caused by chemical attack to vary between 0.4 and 1.0 on different parts of the film. The background density varied less rapidly along the spectra than perpendicular to them.

Tests were carried out in an attempt to simulate the effect of immersion and to try to reproduce the general appearance of the developed flight film. Strips of emulsion were exposed at 2800 Å through a calibrated step wedge and these were developed under identical conditions to the spectrograms. It became apparent that the background density in the spectrograms was not entirely due to contact with seawater, since immersion in seawater resulted in either too little fog or, if left for a period of 5 days or more, in the emulsion peeling off the base material. Since the major part of the spectrograph and the camera housing was fabricated from Mg alloy, it seemed probable that the chemical fog was caused by seawater containing some additional Mg salts. Test strips and lengths of film wound on spools were immersed in seawater solutions containing different parts of Mg alloy. The strips reached the required background densities

after a few days (depending on the Mg concentration) whilst the corresponding times for the film wound on spools was 10–14 days. The latter film had a much closer general appearance to the flight emulsion in terms of density variation across the film than the strips which, as might be expected, had a more uniform background. However, the characteristic H–D curves of the emulsion derived from these two methods were in close agreement at about the same background density.

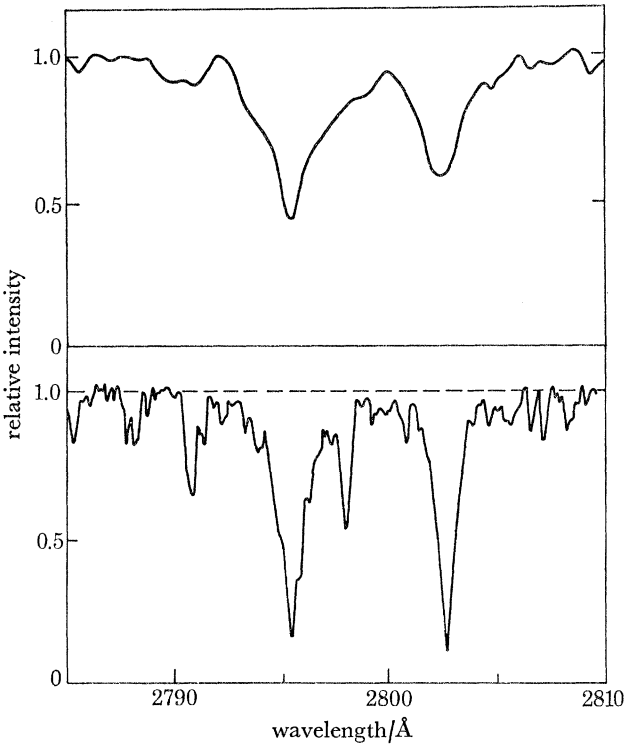

FIGURE 4. Spectra of α Lyr between 2785 Å and 2809 Å: (upper) observed by Lamers *et al.* (1974) and (lower) present data.

The main conclusions drawn from the calibration tests may be summarized as follows:

First, for a given background density due to chemical fog the H–D curves are relatively insensitive to the Mg concentration and the period of immersion prior to development. Spectrum line equivalent width determinations from different calibration curves generally agree within 10%. Secondly, the γ-value of the emulsion decreases as the background fog level increases. Thus, calibration curves are derived to suit the background level in each spectrogram.

As a check for systematic errors in deriving equivalent widths from the emulsion calibration curves, we have compared our values with some TD-1 satellite data obtained by Lamers *et al.* (1974) for α Lyr and Copernicus data by Rogerson *et al.* for λ Sco (1973). A portion of our spectrum of α Lyr between 2785 and 2809 Å is compared in figure 4 with the corresponding portion of the TD-1 data. The higher spectral resolution we obtained enables the Mg II resonance lines to be clearly distinguished from the subordinate lines at 2790.8 Å and 2798.0 Å, and also permits a more accurate estimate of the position of the continuum level. With the continuum placed as shown in figure 4, the total equivalent widths of the four lines is 3.8 Å. This value may be compared with the value 4.1 ± 0.2 Å obtained by Lamers *et al.* (H. J. G. L. M.

Lamers 1974, personal communication). The equivalent widths can be brought into exact correspondence by changing the position of the continuum level in either case by only 1%. In any event, the agreement is highly satisfactory. (A more detailed discussion on the spectrum of this star and the intrinsic stellar spectra of others observed in our joint programme will be published elsewhere.) For λ Sco, from the reported Mg^+ column density derived from a curve of growth analysis for a single cloud model with $b = 6$ cm s^{-1}, we calculate the Copernicus equivalent width for the K line to be 0.22 Å and for the H line, 0.20 Å. These are both approximately 10% greater than our measured mean values but are within our range of uncertainty for this object. Again, the acceptable agreement which we found in this comparison gave us confidence in our emulsion calibration.

Column densities

In determining the equivalent widths of the interstellar lines to derive column densities, particularly the Mg II lines, extreme care had to be taken in accounting for the stellar components in the observed spectra, these being recognizable by their relatively greater breadth and shallower profile than the interstellar components. For Mg II, an attempt was made to use the results of model calculations (Mihalas 1972, and 1973, personal communication) to aid in the definition of the stellar resonance lines by appropriate scaling of the observed nearby subordinate lines. In general this was not successful, but the stellar lines easily could be defined by interpolation through the interstellar components using as a basis the profiles of the subordinate lines. The equivalent widths determined for the Mg II and Mg I interstellar lines for stars from both flights are listed in table 1. The indicated possible errors more reflect systematic uncertainties present in interpretation of the stellar 'continua' than errors of measurement.

In our analysis of the data, we compute individual curves of growth, including radiation damping, for the interstellar medium in line with each star. As a starting point, where possible, we use the multi-cloud velocity profiles obtained from the high-resolution spectral scans of Na I and Ca II by Hobbs and his co-workers (Hobbs 1969; Marschall & Hobbs 1972) as a basis for defining the Mg I and Mg II profiles, assuming a Gaussian distribution of velocities in each of the several cloud components generally evident. The oscillator strengths are from Wiese, Smith & Miles (1969). Of course, the use of these radial velocity parameters is justified only if the line of sight velocity distributions of all the relevant species are similar. According to Hobbs (1973) there is usually good agreement in the kinematics of the various interstellar species, a notable exception being in the gas towards ζ Oph which is quite atypical in this respect. However, in general there are undoubtedly differences between corresponding Na I and Ca II profiles and we would expect there to be differences also between these and the profiles for our observed species. Accordingly, the next step in our procedure is to make small trial adjustments to the initial velocity models and to compute new curves of growth to bring the Mg II H and K doublet column densities into alinement (which, at the outset, generally they are not). This procedure is likely to be more satisfactory than most other analyses which start from the simplifying assumption that, contrary to what is observed, the velocity profile for the gas in line to each star can be described by a single Gaussian. In the course of making our trial adjustments we also are able to identify the sensitivity of the results to the detailed velocity parameters adopted. This is illustrated in figure 5 for δ Ori in which we compare Hobbs's (1969) D_1 profile with four of our trial model profiles. The corresponding curves of

PHILOSOPHICAL TRANSACTIONS OF THE ROYAL SOCIETY A MATHEMATICAL, PHYSICAL & ENGINEERING SCIENCES

TABLE 1. INTERSTELLAR ABUNDANCES AND ELECTRON DENSITY

star s.t. (1)	$E(B-V)$ (2)	distance pc (3)	equivalent width 10^{-3} Å: Mg II K (4)	Mg II H (5)	Mg I (6)	column density cm^{-2}: lg $N(Mg^+)$ (7)	lg $N(Mg^0)$ (8)	lg $N_H^{(a)}$ (9)†	$10^{-5}\frac{N(Mg)}{N_H}$ (10)‡	$10^{3}\frac{N(Mg^+)}{N(Mg^0)}$ (11)‡	electron density $n(e)$ 10^{-3} cm^{-3} (12)‡§	derived H density n_H cm^{-3} (13)‡‖	remarks (14)
γ Ori B2 III	0.01	110	202 (±20)	178 (±20)	60 (±10)	15.23 (+0.38 −0.45)	11.80 (+0.10 −0.10)	19.81 (+0.14 −0.16)	2.7 (+4.4 −2.0)	2.7 (+3.3 −1.9)	3.0 (+3.7 −2.1)	6.0 (+7.4 −4.2)	—
δ Ori 09.5II–III	0.09	340	546 (±20)	479 (±20)	192 (±20)	16.32 (+0.13 −0.12)	12.58 (+0.15 −0.13)	20.11 (+0.15 −0.16)	16 (+15 −7)	5.5 (+4.5 −1.9)	1.5 (+1.2 −0.5)	3.0 (+2.4 −1.0)	several of the cloud regions are common to the lines of sight
ε Ori B0Ia	0.05	360	550 (±30)	480 (±30)	265 (±15)	16.26 (+0.14 −0.18)	12.86 (+0.09 −0.08)	20.24 (+0.15 −0.14)	10 (+10 −5)	2.5 (+1.7 −1.1)	3.2 (+2.2 −1.4)	6.4 (+4.4 −2.8)	
ζ Ori 09.5Ib	0.06	320	570 (+25)	477 (±25)	250 (±20)	16.30 (+0.10 −0.12)	12.90 (+0.12 −0.12)	20.24 (+0.15 −0.14)	11 (+9 −5)	2.5 (+1.7 −1.1)	3.2 (+2.2 −1.4)	6.4 (+4.4 −2.8)	
δ Sco BO.5IV	0.18	170	310 (±50)	235 (±50)	145 (±40)	16.00 (+0.18 −0.22)	14.30 (+0.40 −0.82)	21.12 (+0.14 −0.15)	0.8 (+0.5 −0.4)	50 (+79 −40)	160 (+260 −130)	320 (+520 −260)	dense cloud regions
λ Sco B1.5IV 1	0.02	100	200 (±50)	170 (±50)	⩽10	13.48 (+0.48 −0.48)	⩽10.9	19.90 (+0.20 −0.25)	0.043 +0.090 −0.033	⩾0.37	⩽22	⩽44	case 2 is preferred solution. For $T = 5\times10^3$ K $n(e) \leqslant 3.6 \times 10^{-3}$ cm^{-3}; $n_H \leqslant 7.2$ cm^{-3}
2						15.48 (+0.30 −0.58)	⩽10.9		4.3 (+5.0 −3.6)	⩾37.2	⩽0.22	⩽0.44	
α Vir B1IV 1	0.01	100	125 (±30)	110 (±30)	25 (+15 −10)	13.20 (+0.55 −0.36)	11.35 (+0.25 −0.24)	19.60 (+0.18 −0.24)	0.04 (+0.10 −0.02)	.072 (+0.162 −0.050)	110 (+300 −80)	220 (+600 −160)	case 2 is preferred solution
2						14.81 (+0.50 −0.60)	11.40 (+0.35 −0.29)		1.6 (+3.5 −1.3)	2.5 (+6.6 −1.9)	3.1 (+7.7 −2.4)	6.2 (+15.0 −4.8)	

† These values are referred to in the text.
‡ The errors are the most pessimistic extremes obtained by compounding the errors quoted in columns (7), (8) and (9).
§ These values are derived using parameters assumed for cool interstellar clouds. See text for the details.
‖ This assumes $n(e)/n_H = 5\times10^{-4}$, i..e normal elemental abundances and photoionization by starlight in H I regions.

TABLE 2. PARAMETERS FOR THE INTERSTELLAR CLOUD MODELS

star	cloud	b† km s^{-1}	heliocentric radial velocity km s^{-1}	relative weight‡	remarks
γ Ori	1	2.1	+17.2	0.32	adopted model
	2	2.2	+22.0	0.37	
	3	1.4	+25.6	0.31	
δ Ori (1)	1	1.5	+4.34	0.19	case 1 in figs 5 and 6
	2	2.0	+10.0	0.16	
	3	1.5	+16.0	0.09	
	4	1.0	+21.2	0.03	
	5	1.0	+23.0	0.10	
	6	2.0	+25.6	0.43	
δ Ori (2)	1	2.5	+ 4.34	0.13	case 2 in figs 5 and 6
	2	2.5	+10.0	0.19	
	3	2.0	+16.0	0.11	
	4	1.0	+21.2	0.03	
	5	1.2	+23.0	0.10	
	6	2.0	+25.6	0.44	
δ Ori (3)	1	2.5	+ 4.34	0.13	case 3 in figs 5 and 6
	2	2.5	+10.0	0.19	
	3	2.0	+16.0	0.11	
	4	1.0	+21.2	0.03	
	5	1.2	+23.0	0.10	
	6	2.0	+25.6	0.44	
	7	1.5	+35.0	0.00005	
δ Ori (4)	1	2.5	+ 4.34	0.13	case 4 in figs 5 and 6 The values listed in table 1 are derived from this model
	2	2.5	+10.0	0.19	
	3	2.0	+16.0	0.11	
	4	1.0	+21.2	0.03	
	5	1.2	+23.0	0.10	
	6	2.0	+25.6	0.44	
	7	1.5	+35.0	0.00025	
ε Ori	1	2.22	+ 3.20	0.12	adopted model
	2	0.97	+ 6.14	0.06	
	3	2.05	+11.5	0.22	
	4	2.02	+18.6	0.13	
	5	1.18	+25.0	0.14	
	6	1.73	+28.0	0.25	
	7	1.05	+32.1	0.04	
	8	0.74	+36.7	0.03	
ζ Ori	1	0.80	− 5.93	0.01	adopted model
	2	1.22	− 3.40	0.07	
	3	1.85	− 1.00	0.15	
	4	4.50	+10.8	0.13	
	5	1.10	+18.9	0.06	
	6	1.56	+23.4	0.31	
	7	1.39	+26.3	0.25	
δ Sco	1	1.8	−14.2	0.35	adopted model
	2	1.6	−10.8	0.65	
λ Sco (1)	1	6.0	0.0	1.00	case 1
λ Sco (2)	1	2.6	0.0	1.00	case 2
α Vir (1)	1	4.0	0.0	1.00	case 1 in fig 7
α Vir (2)	1	2.0	0.0	1.00	case 2 in fig 7

† For each cloud component the parameter b is defined by:

$$\psi(u) = \frac{1}{b\sqrt{\pi}} e^{-(u-u_0)/b^2},$$

where $\psi(u)$ is the radial velocity distribution function, u_0 is the central velocity of the cloud.

‡ The relative weight is the proportional number of absorbing atoms of ions in each cloud.

growth are shown in figure 6, and the parameters of these models are listed in table 2. Note that in cases 3 and 4 there is an additional cloud included at a relative velocity of 35 km s^{-1} with relative weights too small for it to be discerned in the Na I or Ca II data. We find that for such clouds to have significant effect on the Mg^+ column densities obtained from the curves of growth they must be relatively unsaturated and well separated in radial velocity from the main cloud structure.

The equivalent widths of the Mg II H and K lines for δ Ori, shown in figure 6, lie off the saturated parts of the various curves of growth and rise up towards the damping parts, the dispersion between the cases being relatively small. This gives us increased confidence in the

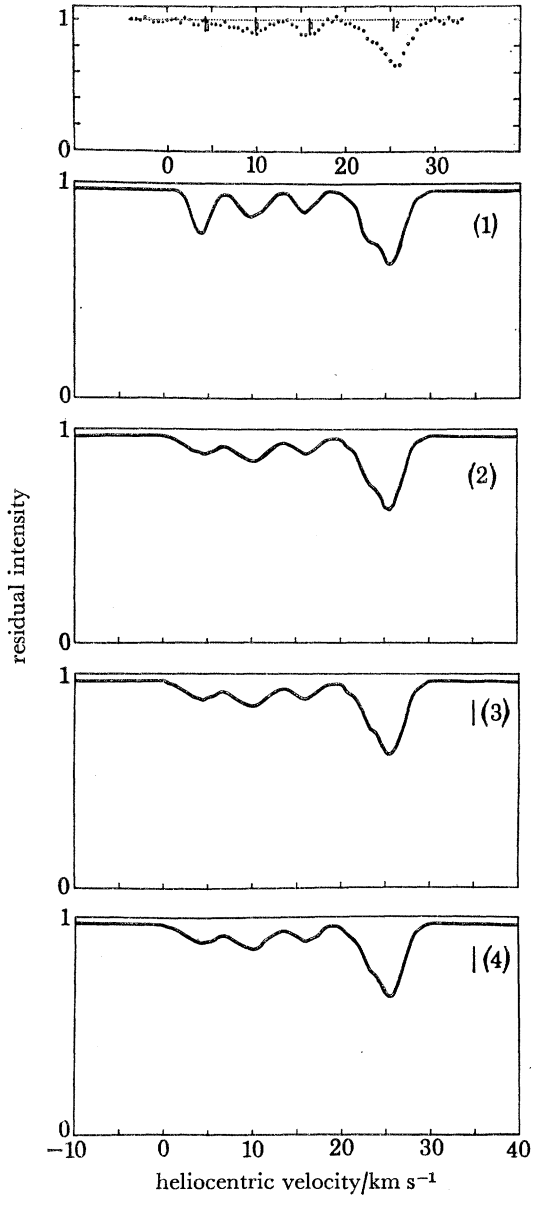

FIGURE 5. Interstellar cloud absorption profiles in the direction of δ Ori. The observed Na I D_1 profile of Hobbs (1969) is reproduced at the top. Various model profiles investigated, having the parameters listed in table 2, are shown below. Small clouds not discernible in the scale of the figure are indicated in the model curves 3 and 4.

derived column densities in spite of the possible lack of accurate knowledge of the actual cloud parameters. We found this to be true in most of the cases we have observed.

The curves of growth for Mg I corresponding to the cases plotted for Mg II also are shown in figure 6 for the typical example δ Ori. Here, the observed value of equivalent width is near the Doppler parts of the various curves of growth, not yet on the saturated parts, and again the dispersion between the cases is relatively small. However, as already mooted, we recognize that Mg^0 may not exist entirely in the same spatial and velocity domains as Mg^+. In particular, Mg^+

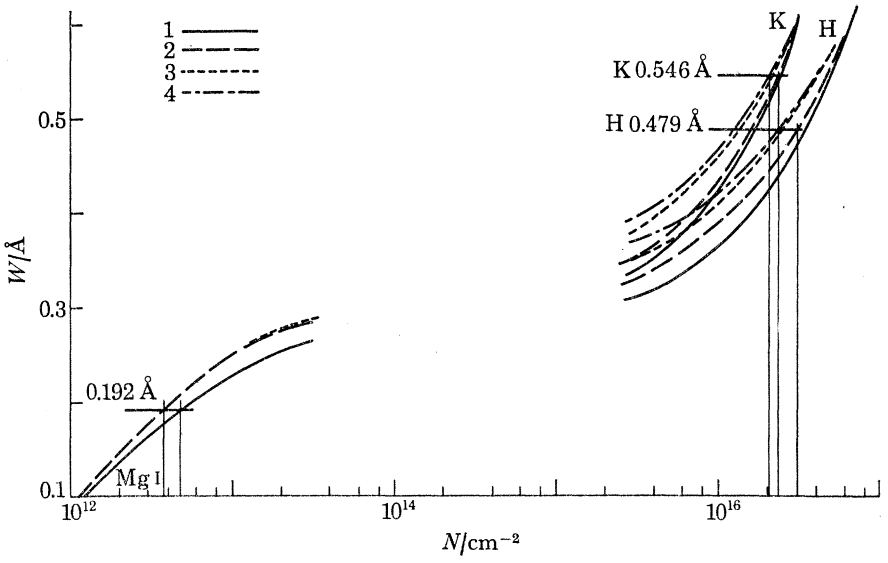

FIGURE 6. Curves of growth for the interstellar gas in the direction of δ Ori corresponding to the model cases illustrated in figure 5. The vertical lines indicate the dispersion in derived column densities for these cases. The adopted values, obtained from the curves giving the best correspondence with the observed doublet ratio for Mg II, are indicated by the thicker vertical lines.

is expected to be present in direct proportion to the local gas density, and Mg^0, to the square of the density. If the relative motions in a given interstellar cloud are large then Mg^+ and Mg^0 may exhibit significantly different radial velocity structures. (Indeed, in deriving the velocity parameters for Mg^+ from Ca^+ and Na^0, which are akin to Mg^0 in this respect, we potentially suffer from this possible shortcoming at the outset. However, our adjustment procedure giving a consistent doublet ratio must improve the fit for Mg^+, and, as already stated, the results then generally turn out to be not very sensitive to velocity profile.) Some simple cases were examined to assess the likely magnitude of the effect. A cloud rotating as a solid gives no Doppler spreading in any line of sight through it. A differential rotator, on the other hand, does give a Doppler spreading. As a trial case we assumed a homogeneous optically thin cloud in which the Mg^+ density is proportional to the reciprocal of the radius and Mg^0 to the reciprocal of its square. The dispersion in radial velocities between Mg^+ and Mg^0 derived for several values of total density and radius indicated that gross rotational motion of a cloud is unlikely to be a significant contributer in the context of the observed velocity profiles. This points to small-scale turbulence as the dominant local velocity mechanism and implies that within a cloud Mg II and Mg I lie on curves of growth having essentially the same velocity parameters. However, different clouds (or absorbing regions generally) in line of sight to a star may ave different ionization conditions, and the absorptions due to Mg^+ and Mg^0 in spatially

uncorrelated regions then will have different relative weightings, and in turn their curves of growth will not have entirely the same velocity parameters. Nevertheless, since we observe the Mg I line generally not to be saturated our Mg^0 column densities are unlikely to be grossly in error. We return to this discussion later.

Our column densities for seven stars are listed in columns 7 and 8 of table 1. Details of the adopted velocity parameters are given in table 2. The possible errors in our derived column densities are difficult to assign; the indicated uncertainties were judged for each result only on the basis of the systematic uncertainties in equivalent width. The results for γ, δ, ε and ζ Ori and δ Sco are based on cloud models obtained from the Na I or Ca II profiles of Hobbs & Marschall and Hobbs, adjusted to conform with our observed Mg II doublet ratios. Unfortunately, there are no high resolution interstellar line profiles available for λ Sco or α Vir; for these cases we assumed a single Gaussian velocity profile and again adjusted the b parameter in the curves of growth to give the observed Mg II doublet ratios. Two possible solutions for b then exist for each case: 2.6 km s^{-1} or 6.0 km s^{-1} for λ Sco and 2.0 km s^{-1} or 4.0 km s^{-1} for α Vir.

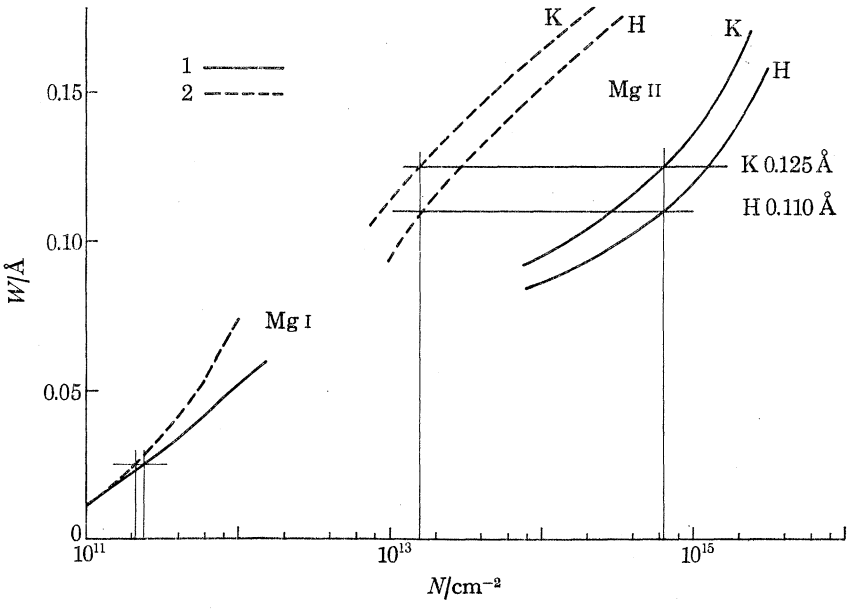

FIGURE 7. Curves of growth for the interstellar gas in the direction of α Vir corresponding to the model cases (1) and (2) listed in table 2.

The curves of growth for α Vir are shown in figure 7. The corresponding column densities for both solutions are listed in table 1. It is evident that the derived Mg^0 values in line to these stars are quite insensitive to the choice of b, but the Mg^+ values depend strongly on b.

Also listed in table 1 are the values of total hydrogen column density N_H ($= N(H\,I) + 2N(H_2)$) from Savage & Jenkins (1972), Jenkins & Savage (1974), Spitzer *et al.* (1973) and Smith (1973). The resulting values of derived interstellar Mg abundance (assumed to be predominantly Mg^+) relative to hydrogen are listed in column 10. These values do not depend significantly on the ionization state of the medium and fundamentally are average values along the lines of sight. For comparison, the cosmic abundance of Mg relative to hydrogen is 3.5×10^{-5} by number (Withbroe 1971).

Our derived relative Mg abundance for γ Ori is close to the cosmic value, for the Belt stars δ, ε and ζ Ori is a few times higher, and for δ Sco is a few times lower. Our value is also close to cosmic for the case $b = 2.6$ km s^{-1} for λ Sco and only a factor 2 lower for the case $b = 2.0$ km s^{-1} for α Vir. The alternative cases for these two stars give values lower than the cosmic value by nearly a factor 100.

Electron densities

We assume that the process of ionization is due to the general stellar photon radiation field and that recombination occurs by collisions between ions and free electrons. The relative numbers of singly ionized and neutral Mg atoms then are given by

$$\frac{n(\mathrm{Mg^+})}{n(\mathrm{Mg^0})} = \frac{\Gamma(\mathrm{Mg^0})}{\alpha_{\mathrm{tot}}(\mathrm{Mg^0})\, n(\mathrm{e})}, \tag{1}$$

where $n(\mathrm{Mg^+})$ and $n(\mathrm{Mg^0})$ are the respective number densities, $n(\mathrm{e})$ is the number density of electrons, $\Gamma(\mathrm{Mg^0})$ is the photoionization rate per atom in units s^{-1} and $\alpha_{\mathrm{tot}}(\mathrm{Mg^0})$ is the total recombination coefficient in units cm^3 s^{-1}. The value of $\Gamma(\mathrm{Mg^0})$ is given by

$$\Gamma(\mathrm{Mg^0}) = 10^{-8}\, h^{-1} \int_{\lambda_0}^{0} a(\lambda)\, u(\lambda)\, \lambda\, \mathrm{d}\lambda, \tag{2}$$

where h is Planck's constant, λ is a wavelength expressed in Å, $a(\lambda)$ is the photoionization cross-section for $\mathrm{Mg^0}$, $u(\lambda)$ is the interstellar radiation density and λ_0 is the photoionization threshold, at 1618.4 Å. We assume for H I regions that $u(\lambda) = 0$ at $\lambda < 912$ Å.

We used the data of Witt & Johnson (1973) for $u(\lambda)$ appropriate for the solar vicinity, and of J. Dubau & J. B. Wells (1974, personal communication) for $a(\lambda)$. The radiation density calculations by Witt & Johnson are based on recent satellite observations and give values about a factor 2 higher than earlier calculations by Habing (1968) over the wavelength range of interest here. The result terminates before 912 Å, at 1250 Å, and we extrapolated linearly to zero at 912 Å. The photoionization cross-section was computed by Dubau & Wells using atomic wave functions obtained in Seaton & Wilson's (1972) frozen cores approximation. The resulting value of $\Gamma(\mathrm{Mg^0})$ is 8×10^{-11} s^{-1} (this is a revised value, about 50 % larger than in our previous publications).

The recombination coefficient $\alpha_{\mathrm{tot}}(\mathrm{Mg^0})$ is the sum of the radiative and dielectronic coefficients obtained respectively from Peach (1974, personal communication; and 1967) and Aldrovandi & Péquignot (1973). We plot these contributions individually as a function of temperature in figure 8. At a gas temperature of 60–70 K, which we assume to be typical of interstellar clouds, $\alpha_{\mathrm{tot}}(\mathrm{Mg^0}) = 1.0 \times 10^{-11}$ cm^3 s^{-1}. This is also the value at 10^4 K. Near 5×10^3 K $\alpha_{\mathrm{tot}}(\mathrm{Mg^0})$ has a minimum value of about 6×10^{-13} cm^3 s^{-1}.

For the ratio $n(\mathrm{Mg^+})/n(\mathrm{Mg^0})$ we take $N(\mathrm{Mg^+})/N(\mathrm{Mg^0})$, the ratio at column densities; again, the implicit assumption is that the space distributions of $\mathrm{Mg^+}$ and $\mathrm{Mg^0}$ largely correspond. We assume further that the interstellar gas is mainly concentrated into cool clouds at temperature 60–70 K. Values of $n(\mathrm{e})$ corresponding to these assumptions are listed in column 12 in table 1.

Discussion

Our values for the relative Mg abundance for the material averaged along the lines of sight to the Belt stars δ, ε and ζ Ori are self-consistent and a few times higher than the cosmic value 3.5×10^{-5}. In the direction to γ Ori our value is very close to cosmic and in the dense regions to δ Sco, is a few times lower. In the cases of λ Sco and α Vir the uncertainty about the correct velocity dispersion for the absorbing regions makes definite conclusions concerning the state of the material towards these stars rather tentative. The *Copernicus* observations of Rogerson *et al.* (1973) led them to adopt the value $b = 6$ km s^{-1} for a single cloud model in the case of

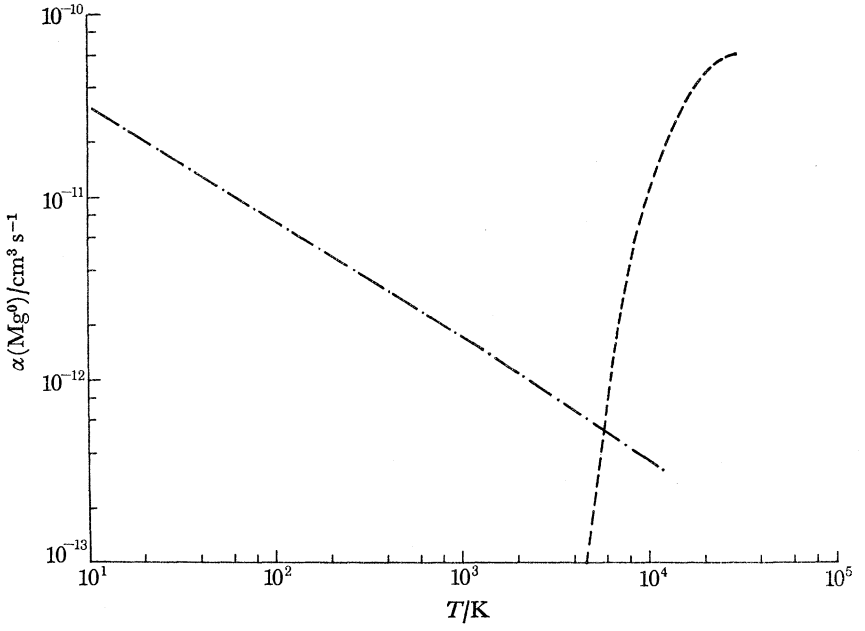

Figure 8. Recombination coefficients plotted against temperature for $Mg^+ \rightarrow Mg^0$. – – –, radiative recombination coefficient, $\alpha_{rad}(Mg^0)$; – –, dielectric recombination coefficient, $\alpha_{diel}(Mg^0)$. $\alpha_{tot}(Mg^0) = \alpha_{rad}(Mg^0) + \alpha_{diel}(Mg^0)$.

λ Sco. We note that the column density of Mg^+ they report is within the range of uncertainty of the value we obtain using the same b value; this choice, however, yields a figure for the relative Mg abundance that is low by a factor 100. On the other hand, the figure obtained by choosing the alternative solution $b = 2.6$ km s^{-1} gives a value in good agreement with the cosmic value. Similarly, for α Vir, the simplified cloud model yields two solutions for the b parameter: 4.0 and 2.0 km s^{-1}. The former again gives for the relative Mg abundance a value 100 times lower than cosmic, while the latter gives a value within a factor 2. We see no reason why the solutions consistent with the cosmic value of Mg abundance should not be appropriate. Indeed, we have a positive preference for these values, as will be made clear in the following discussion on electron density.

We note that for the Orion stars our derived values of n(e) do not deviate much from their mean near 3×10^{-3} cm^{-3}. For α Vir n(e) also is close to 3×10^{-3} cm^{-3} in the case $b = 2.0$ km s^{-1}. α Vir is a distance of about 100 pc and is situated out of the Galactic plane; a single cloud model as we assume for the gas in line to this star then may be reasonable and, if it is so, the value $b = 2.0$ km s^{-1} is more likely than 4.0 km s^{-1} since it is typical of the individual cloud

profiles in Hobbs's data. For δ Sco, at a distance of 170 pc, the large value of n(e) found in this case (0.16 cm^{-3}) is consistent with the high cloud density as is implied in the large values for E(B–V) and N_H. For λ Sco, Mg^0 is undetectable and only an upper limit is obtained. In the case $b = 2.6$ km s^{-1} the limit on n(e) derived under the previously stated assumptions then is apparently about a factor 10 lower than for the Orion stars. On re-application of equation (1) with α_{tot}(Mg^0) now as an adjustable parameter we obtain an upper limit value for n(e) near the mean for the Orion stars, at a gas temperature of a few thousand kelvins. This result points to the existence of a cloud-like H I region in line to λ Sco at a much higher temperature than the normal cool clouds. The observations are not easily explained by an intercloud region having the high value of n(e) derived from pulsar dispersion measures.

Assuming that ionization by starlight of photon energy < 13.6 eV is the process chiefly responsible for the observed values of n(e), we expect $n(e)/n_H \approx 5 \times 10^{-4}$ for normal elemental abundances, where n_H is the number density of H. Using this to obtain n_H from the values of n(e) listed in table 1 gives the quantities in column 13. We note that the resulting values for the Orion stars are consistent with the expected density of interstellar clouds. The high cloud density found for δ Sco again simply reflects the large values for E(B–V) and N_H. For α Vir, however, the large value for n_H corresponding to the case $b = 4.0$ km s^{-1} is inconsistent with its unreddened character and small N_H, and again the case $b = 2.0$ km s^{-1} gives a more reasonable value, similar to those for the Orion stars. On the other hand, for λ Sco, the case $b = 2.6$ km s^{-1} giving a normal Mg abundance leads to $n_H < 0.22$ which is rather small for a cool cloud component if the values listed for the other lightly reddened stars are typical. In fact, if H were evenly distributed to λ Sco n_H would be 0.26 cm^{-3}. However, as in the previous discussion on n(e), in terms of our simple model, if we assume a higher gas temperature then the derived value for n_H is raised: for a temperature of 5×10^3 K, $n(e) \leqslant 3.6 \times 10^{-3}$ cm^{-3} and $n_H \leqslant 7.2$ cm^{-3}. Nevertheless, these being upper limit values the implication still is that the absorbing region in line to λ Sco is more tenuous than to the other stars observed. If so, it is likely also to be more extended. Thus we suggest that there is an interstellar region in the direction of λ Sco that is quite unlike those to most of the other stars listed in table 1, namely a hot, extended cloud of rather low density. Contrasting this is the region in line to δ Sco which contains cool clouds of high density.

An important outcome of our derived values for n(e) and n_H is the fact that they are entirely consistent with the supposition that photoionization by starlight is the only significant ionizing mechanism in interstellar clouds. At the risk of stating the obvious, the fact that photoionization is assumed in consideration of the ionization balance of Mg$^+$ and Mg^0 does not lead circularly to this conclusion. If cosmic rays or X-rays play a role in ionizing Mg then hydrogen also would be partially ionized giving much higher values of n(e) then we have derived.

Finally, returning to the question of the space distributions of Mg$^+$ and Mg^0, with the exception of the special cases δ and λ Sco, the remarkably consistent values for N(Mg$^+$)/N(Mg^0) we obtain points to the validity of our assumption that Mg$^+$ and Mg^0 are correlated in interstellar clouds.

It is a pleasure to acknowledge the support and encouragement of Sir Harrie Massey, Sec.R.S., Professor D. J. Bradley and Professor H. B. Gilbody. We gratefully thank our colleagues at U.C.L. and Q.U.B., especially T. E. Venis, W. A. Towlson, S. McC. Noble and D. Wilkinson, whose participation has made these observations possible. Thanks are due also

PHILOSOPHICAL TRANSACTIONS OF THE ROYAL SOCIETY A MATHEMATICAL, PHYSICAL & ENGINEERING SCIENCES

to Y. Kondo of Nasa Manned Spacecraft Center and Professor R. Wilson of U.C.L. (then of the S.R.C. Astrophysics Research Unit, Culham Laboratory) for helpful discussions and the use of laboratory facilities, and to the personnel at N.C.A.R., Palestine, for launch and recovery operations and general hospitality. Financial support from the Science Research Council was gratefully received.

References (Boksenberg *et al.*)

Aldrovandi, S. M. V. & Péquignot, D. 1973 *Astron. & Astrophys.* **25**, 137.
Boksenberg, A., Kirkham, B., Towlson, W. A., Venis, T. E., Bates, B., Courts, G. R. & Carson, P. P. D. 1972 *Nature Phys. Sci.* **240**, 127.
Boksenberg, A., Kirkham, B., Towlson, W. A., Venis, T. E., Bates, B., Courts, G. R. & Carson, P. P. D. 1974 *Space Res.* **14** (in the Press).
Habing, H. J. 1968 *Bull. astr. Insts Neth.* **19**, 421.
Hobbs, L. M. 1969 *Astrophys.* **157**, 135.
Hobbs, L. M. 1973 *Astrophys. J.* **180**, L79.
Jenkins, E. B. & Savage, B. D. 1974 *Astrophys. J.* **187**, 243.
Lamers, H. J., van der Hucht, K. A., Hoekstra, R., Faraggiana, R. & Hack, M. 1974 *Space Res.* **14** (in the Press).
Marschall, L. A. & Hobbs, L. M. 1972 *Astrophys. J.* **173**, 43.
Mihalas, D. 1972 *Astrophys.* **177**, 115.
Peach, G. 1967 *Mem. R.A.S.* **71**, 13.
Rogerson, J. B., York, D. G., Drake, J. F., Jenkins, E. B., Morton, D. C. & Spitzer, L. 1973 *Astrophys. J. Lett.* **181**, L110.
Savage, B. D. & Jenkins, E. B. 1972 *Astrophys. J.* **172**, 491.
Seaton, M. J. & Wilson, P. M. H. 1972 *J. Phys.* B **5**, 11.
Smith, A. M. 1973 *Astrophys. J.* **179**, L11.
Spitzer, L., Drake, J. F., Jenkins, E. B., Morton, D. C., Rogerson, J. B. & York, D. G. 1973 *Astrophys. J.* **181**, L116.
Wiese, W. L., Smith, M. W. & Miles, B. M. 1969 *NSRDS–NBS22* **2**, 1.
Withbroe, G. L. 1971 *The Menzel Symposium* (NBS Special Public. 353), ed. K. B. Gebbie, Washington: U.S. Government Printing Office.
Witt, A. N. & Johnson, M. W. 1973 *Astrophys. J.* **181**, 363.

PHILOSOPHICAL TRANSACTIONS OF THE ROYAL SOCIETY A MATHEMATICAL, PHYSICAL & ENGINEERING SCIENCES

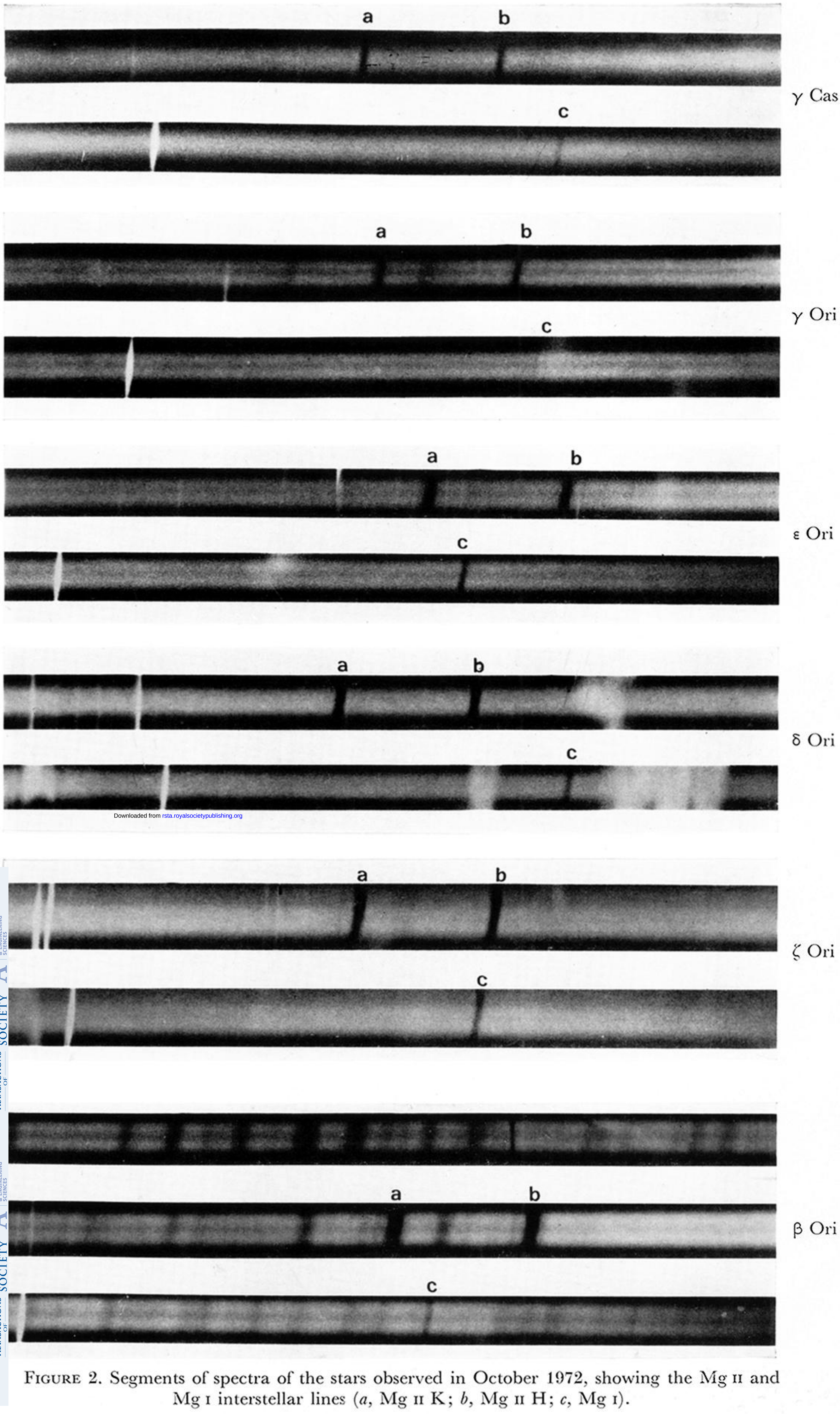

FIGURE 2. Segments of spectra of the stars observed in October 1972, showing the Mg II and Mg I interstellar lines (*a*, Mg II K; *b*, Mg II H; *c*, Mg I).

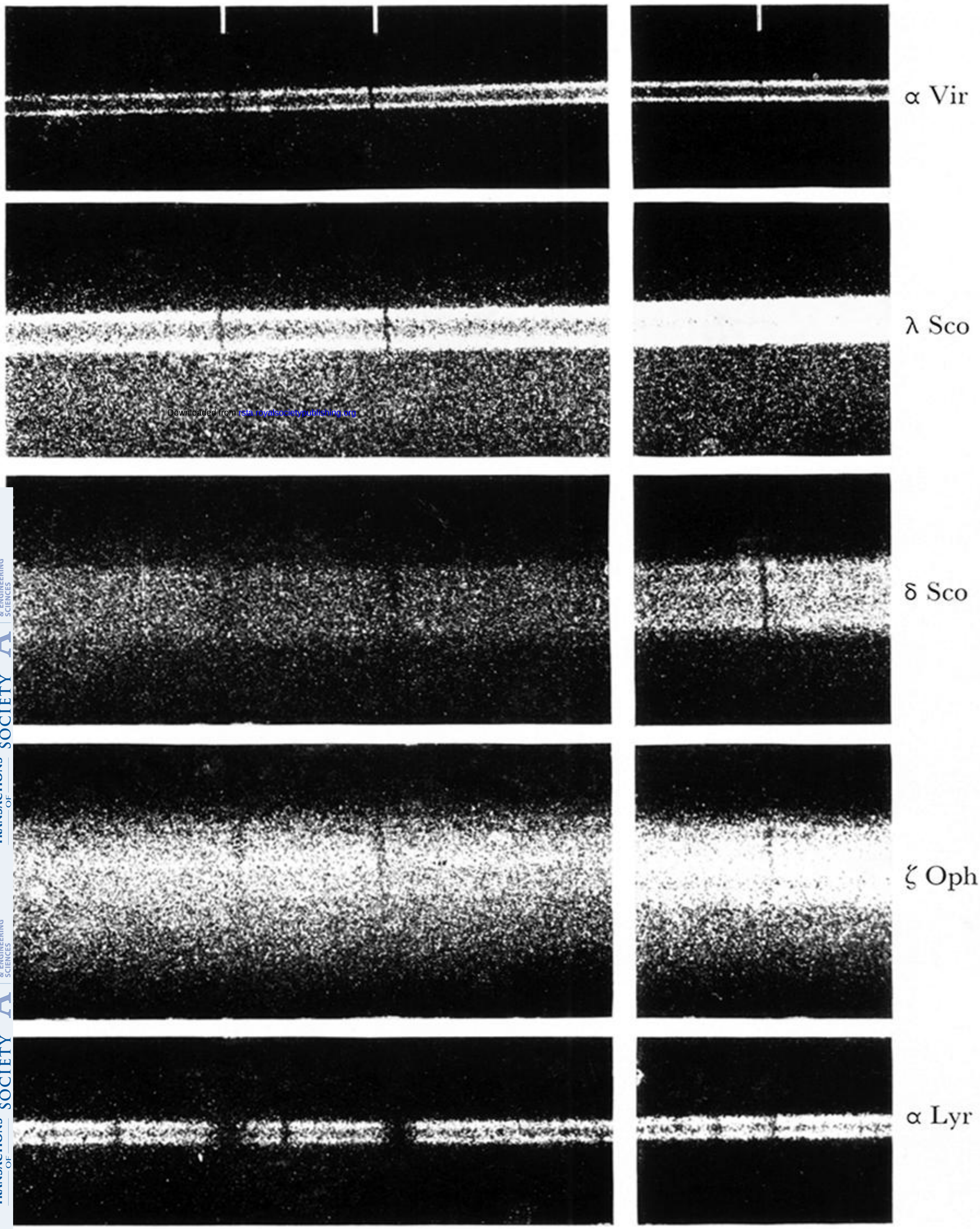

PHILOSOPHICAL TRANSACTIONS OF THE ROYAL SOCIETY A MATHEMATICAL, PHYSICAL & ENGINEERING SCIENCES

FIGURE 3. Segments of spectra of the stars observed in May 1973.